Sensitivity analysis of the uncertainties of the mechanical design parameters: Stochastic study performed via a numerical design of experiment

Ghinwa Ouaidat, Abel Cherouat, Raed Kouta, Dominique Chamoret

Sensitivity analysis of the uncertainties of the mechanical design parameters: Stochastic study performed via a numerical design of experiment

Ghinwa Ouaidat[a,b,*], Abel Cherouat[a], Raed Kouta[b], Dominique Chamoret[c]

a. University of Technology of Troyes-GAMMA3, 12 rue Marie Curie, 10004 Troyes, France
b. University of Technology of Troyes-M2S, 12 rue Marie Curie, 10004 Troyes, France
c. ICB UMR 6303, CNRS, UBFC, University of Technology of Belfort-Montbéliard, 90010 Belfort, France

ghinwa.ouaidat1@gmail.com, abel.cherouat@utt.fr , raed.kouta@utbm.fr, dominique.chamoret@utbm.fr

*: *corresponding author*

Abstract

As the GDL (Gas diffusion layer) is the most sensitive component in the fuel cell, any change in its structure causes a change in its porosity, which strongly influences the contact between the components of the fuel cell. Note that the state of contact depends on the applied clamping pressure, the thickness and the porosity of the GDL, and the geometry of the rib (bending radius) of the BPP (Bipolar plates). These components can be subject to variations coming from very high compression, so it is necessary to consider the reliability of their dimension via modeling/simulation by the integration of uncertainties. In this article, we will study the influence on the contact pressure of the uncertainties of the mechanical design parameters. A probabilistic approach (Gauss's law) is applied to evaluate the effect of the mechanical uncertainties parameter on the contact pressure between GDL/MEA and GDL/BPP.

Keywords: PEMFC, Statistical analysis, Design of Experiments, Contact Pressure.

1 Background and Issues

The majority of research projects that are of more importance are those that are oriented towards an industrial field, particularly the automobile. In this field, one of the many

technological advancements to be achieved is that of Proton Exchange Membrane Fuel Cell (PEMFC) fuel cells used in the transportation field where hydrogen is the best solution as a non-polluting, sustainable and renewable energy source. The PEMFC is characterized by their low operating temperature which allows a fast-cold start according to the reverse principle of water electrolysis. Moreover, is also characterized by their strong power density and a very high energy performance.

PEMFCs are designed and built on an assembly of heterogeneous components (in terms of materials and dimensions), mechanically maintained and also subjected to potentially strong constraints. Multiple coupled phenomena: mechanical, electrical, thermal and fluidic occur during the transformation of hydrogen fuel into electrical energy related to the conditions of use that can lead to degradations impacting the lifespan and reliability [1], [2], [3], [4] and [5].

Therefore, the fuel cell performance depends on different parameters:

- Operational: temperature and mechanical clamping pressure
- CAD design : dimensions and geometry of the components
- Material : mechanical and physical properties of each component

This performance can be reduced in time due to the materials and the assembling degradation [6] and [7]. The mechanical effects occurring at the heart of the fuel cell influence also the lifetime of different PEMFC components [8] and [9].

As the fuel cell is a complex system, durability and reliability remain an important stake in the design, manufacturing and optimization of fuel cell system.

For example, in the transport field the durability of the fuel cell is an important problem that constitutes an obstacle to its commercial development. In fact, the fuel cell has a limited lifetime (2500 hours), while a lifetime of 5000 hours would be necessary for marketing in the automotive field. This goal is not achieved if we consider the autonomy of current prototypes. The failure is mainly due to the miss of control of random physical phenomena taking place inside the cell. These phenomena are, in large part, due to the uncertainties of the thermal parameters of the cell (temperature, relative humidity, etc.) and affect the performance of the cell and thus that of the entire stack. It therefore appears necessary to have a reliability model to predict the performance and endurance of the PEMFC.

A greater reliability requires better knowledge of the impact of uncertainties operating and mechanical parameters related to the design and manufacture of the PEMFC. Several recent

numerical studies show the influence of the uncertainties of several operating parameters on the performance of the PEMFC system:

- Vlahinos, A. *et al.* [10] have developed a probabilistic finite element method by varying the input parameters according to a Gauss law. They studied the effect of material variations, such as the Young's modulus and the thickness of the bipolar plate, the thickness of the membrane and the mechanical load of the bolt on the uniformity of pressure distribution on two parts of the membrane: above and in the middle of the MEA. The obtained results show that the maximum and differential compression stresses at the top of the membrane are approximately 13% higher than the values of the stresses in the middle.
- Placca, L. *et al.* [11] have studied the effect of different degradation rate of the active surface of the membrane on the lifetime of the fuel cell for different temperatures and over variable operating times. These three factors are considered random and defined by their average and standard deviation. A random factorial experimental design was made consisting of six two-level parameters. After analyzing the effects of the factors on cell voltage, the authors found that the temperature has the most effect on dispersion.
- Noguer, N. *et al.* [12] have developed a knowledge model to study the influence of the uncertainties operating parameter on fuel cell voltage. They studied the influence of the normal law random variation of the porosity of the GDL on the fuel cell voltage. The obtained results show that the increase in the dispersion of the porosity of the GDL from 1% to 10%, leads to a distribution of the voltage of the cell. This distribution law of the fuel cell voltage is physically related to the limit imposed by the diffusion of the reactive gases in the heart of the fuel cell.
- Mawardi, A. *et al.* [13] have developed a non-isothermal 1D stochastic model to analyze the uncertainty effect of nine operating parameters such as cell temperature, anode and cathode parameter (pressure, humidity, stoichiometry, molar fraction in gas) on the PEMFC performance. The authors show that a stochastic convergence analysis with 100 simulations is sufficient to achieve acceptable results.
- Zhang, W. *et al.* [14] have studied the influence of seven parameters (Young's modulus and thickness of the end plate and the MEA, the position and the pressure of the bolts) on the distribution of the mechanical stresses. The authors show that the position of a bolt has a major influence on the maximum stresses of the bipolar plate

and the end plate. However, the thickness of the end plate has the strongest effect on the maximum stress of the MEA. For the end plate, there are two sensitive parameters which are the positions of the bolts. In addition, the results show that the material properties of the end plate and the pressure of the bolts are two main factors that influence the maximum stress of BPP.

- Akiki, T. [15] has applied uncertainties on two parameters (material of the bipolar plate and clamping pressure) for three shapes of the rib of the bipolar plate (rectangular, trapezoidal and trapezoidal with bending radius). These two parameters follow a normal law of average 0 and standard deviation of 0.1. The obtained results show that the porosity of the GDL is greater in the case of trapezoidal geometry with a bending radius than in the case for the rectangular and the trapezoidal.

Most of the previous studies have focused on the physicochemical phenomena and have shown that the performance of the PEMFC is strongly influenced by the operating conditions such as temperature, pressure, anode and cathode stoichiometry coefficients, and the degradation rate of the active surface of the membrane.

However, experiments on fuel cell have shown the influence of structural parameters such as the thickness of the GDL and the electrolyte, the porosity of the GDL and the geometry of the components and in particular the geometry of the RIB of the bipolar plate (BPP). The influence of geometrical/mechanical parameters related to PEMFC components on the behavior and electrical performance of the assembly is performed with the integration of uncertainties related to the mechanical design parameters and the materials properties.

However, the study of the effect of the uncertainties parameters on the performance of the cell and in particular the distribution of the contact pressure between each fuel cell components is not well understood due to the little literature on mechanical aspects.

The contact pressures sustained by the GDL will directly impact the electrical performance of the fuel cell. Therefore, our attention was focused on the contact pressure distribution between GDL/BPP and GDL/MEA.

In this paper, the influence on the distribution of contact pressure of the uncertainties of the mechanical design parameters is study numerically. Deterministic model developed in [16] is used to simulate of the behavior of the fuel cell, in particular the contact pressure, from determined and constant parameters. The effect of the uncertainties parameters on the

performance of the cell and in particular the distribution of the contact pressure between each fuel cell components is analyzed.

Due to the geometrical symmetry of the cell, a stack of three cells is modeled in 2D. Our model consists of a stack of three cells of MEA, a bipolar plate, a GDL to end with an endplate (figure 1a). To model the clamping force on the plate, a clamping pressure of 1 MPa in the direction y is applied on the top of the End plates. The other boundary conditions are specified in figure 1a. A contact with friction of a coefficient μ=0.3 is defined between the different components (Coulomb's Law). In this study the mechanical behavior of all components is assumed to be linear isotropic.

The obtained numerical simulations of a stack of three cells under mechanical compression show that the distribution of contact pressure under the rib of the bipolar plate (BPP) (Figure. 1a) in each cell is the same. The following physical phenomena that we can noting are:

1. The contact pressure between GDL/BPP is distributed uniformly (C_{press} = 1.77 MPa) under all the rib of the bipolar plate (figure.1b).
2. Under the BPP channel, a zero contact pressure is observed corresponding to the separation between the GDL and the MEA.
3. The maximum contact pressure is located at the GDL detachment point from the bipolar plate, which generates peak pressures at the detachment point. We can also see that this maximum contact pressure occurs at the rib D_2 and D_4 (2.83 MPa), however a maximum contact pressure of 2.18 MPa is observed under the rib D_1, D_3 and D_5 (2.18 MPa). This little interval between the maximum contact pressures does not affect the electrical contact resistance results between GDL/BPP.
4. The increase in the number of cells and the number of the rib of the bipolar plate does not influence the distribution of contact pressures between GDL/BPP under all the rib of the bipolar plate. Therefore, we considered a cell with one rib (D_3) instead of a stack of multi-rib cells.

Taking into account the results below, only one half-channel and rib of the cell are modeled in 2D. This article is organized as follows: in section 2, we present the deterministic model as well as the results obtained on the relationships between the mechanical parameters and the contact pressure between the components. In the third section, we study the influence on the distribution of contact pressure of the uncertainties of the mechanical design parameters.

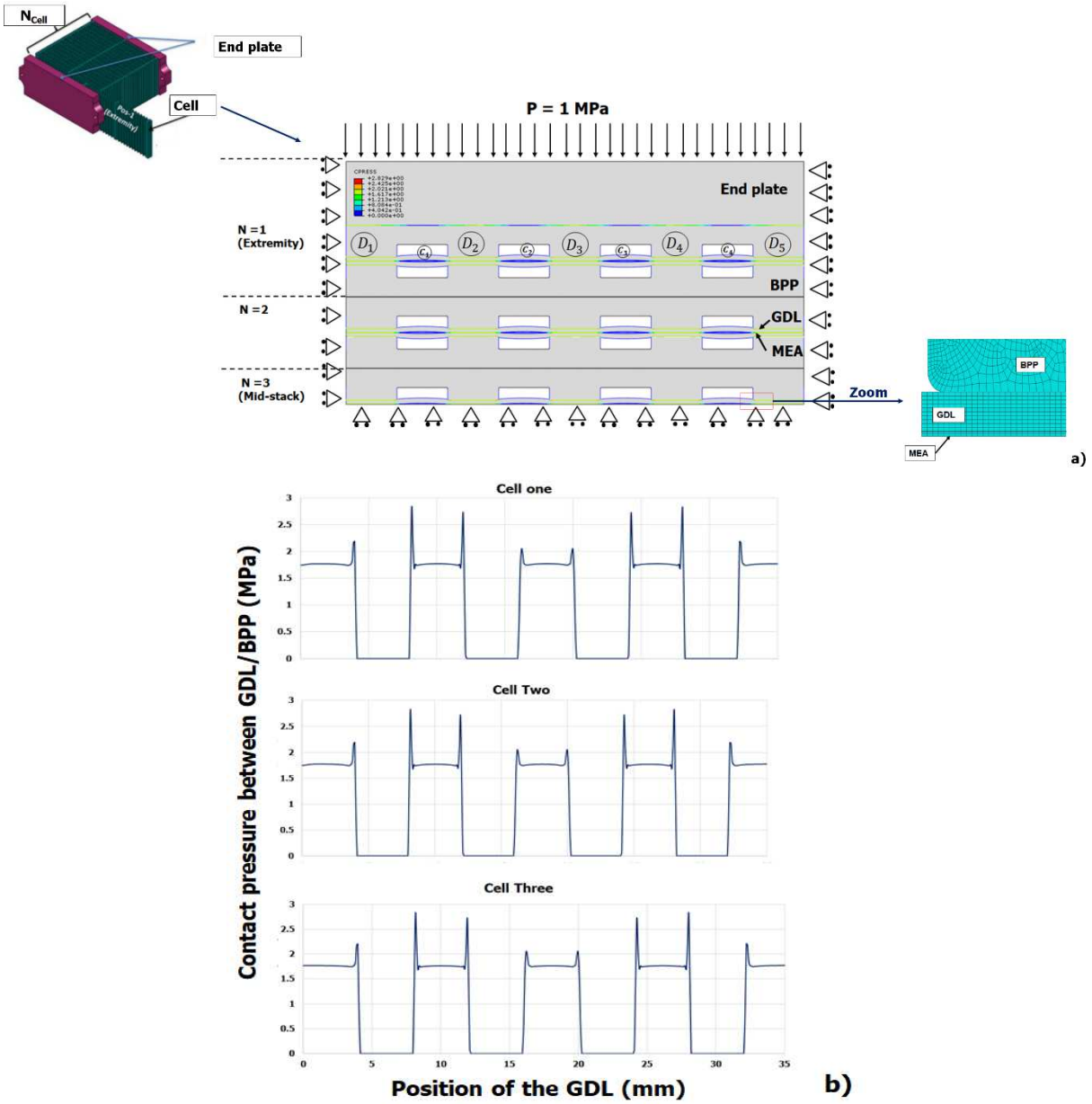

Figure 1: a) stack of 3 cells; b) Distribution of the contact pressure between GDL/BPP all along the GDL line for the 3 cells.

2 Deterministic model

A deterministic model [16] based on the mechanical parameters associated to the Design of Experiments and ANOVA and finite element analysis is performed to determine the relationship between the design parameters and the contact pressure. The parameters retained in our study are the porosity of the GDL and the thickness of the GDL (T_{GDL}) and the bending radius of the bipolar plate (R_{RIB}). The porosity modeling is based on a homogenized approach of the GDL with an equivalent Young's modulus [E_{eqv}] (see Figure 2).

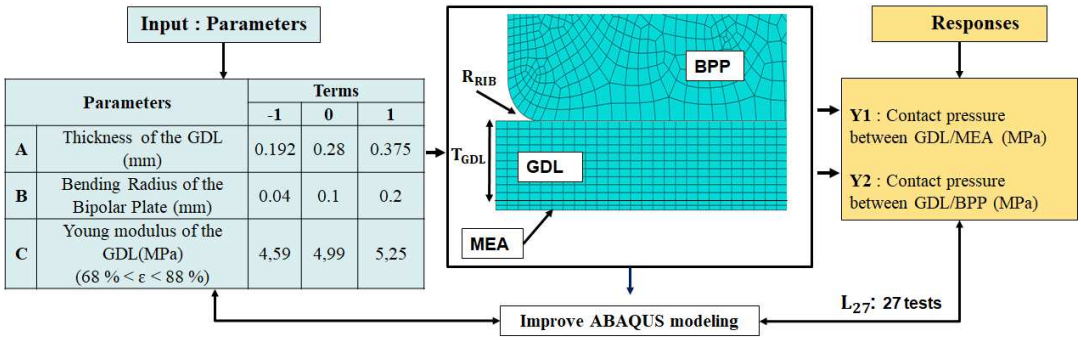

Figure 2: Terms of the input studied parameters and responses

The results obtained showing the relationship of these parameters (A, B and C) with the contact pressures GDL/MEA (Y_1) and GDL/BPP (Y_2) are illustrated by Equations 1 and 2:

1. Contact pressure between GDL/MEA :

$$Y_1 = 1.05 - 0.0105A + 0.03B - 0.004AB + 0.011B^2 \quad (1)$$

2. Contact pressure between GDL/BPP :

$$Y_2 = 1.737 + 0.124A - 0.249B + 0.0205C + 0.021B^2 - 0.046AB^2 - 0.0113BC + 0.02425B^2C \quad (2)$$

The results of the design of experiments allow us to identify the ideal parameters for optimal PEMFC performance: thickness of the GDL T_{GDL}= 0.375 mm, R_{RIB} = 0.04 mm and Young's modulus of the GDL E_{eqv} = 4.59 MPa corresponding to a porosity of 88 %. From these parameters, we were able to determine the variation of the interfacial resistance between GDL/BPP as a function of the clamping pressure. The interfacial contact resistance (R) is calculated by Equation 3:

$$R = \frac{A}{S} * \left(\frac{B}{P}\right)^{\beta} \quad (3)$$

Where *S* is the contact surface of the interface, *P* is the contact pressure between GDL/Bipolar plate and A, B and β are characteristic parameters of the type of the bipolar plate and the GDL determined by experiences [17].

The numerical results of the contact resistance versus the clamping pressure were compared to experimental results (Figure 3). The decrease in the interfacial electrical resistance between the GDL/BPP leads to an increase in conductivity.

The obtained results allowed to identify three optimal parameters from the Design Of Experiments and may be subject to variation resulting from the deformation of the bipolar plate, the membrane and the GDL and the changing the electrical contact resistance.

Numerical design of experiments is then used to predicate the fuel cell behavior under mechanical clamping pressure the by integrating the obtained uncertainties optimal parameters.

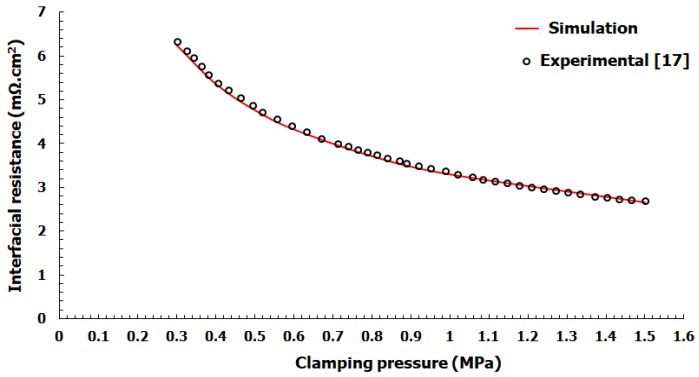

Figure 3: Contact resistance versus clamping pressure comparison numerical model and experimental results [16-17]

3 Study of the influence of uncertainties and performance.

Statistical analysis is used to integrate the uncertainties of parameters in the deterministic model with different statistical distribution (Normal, Uniform, Log-Normal, Beta, Weibull and Gamma law) [25-26-27]. Figure 4 shows the distributions applied to the input parameters as well as the dispersions observed and the consequences on the outputs parameters.

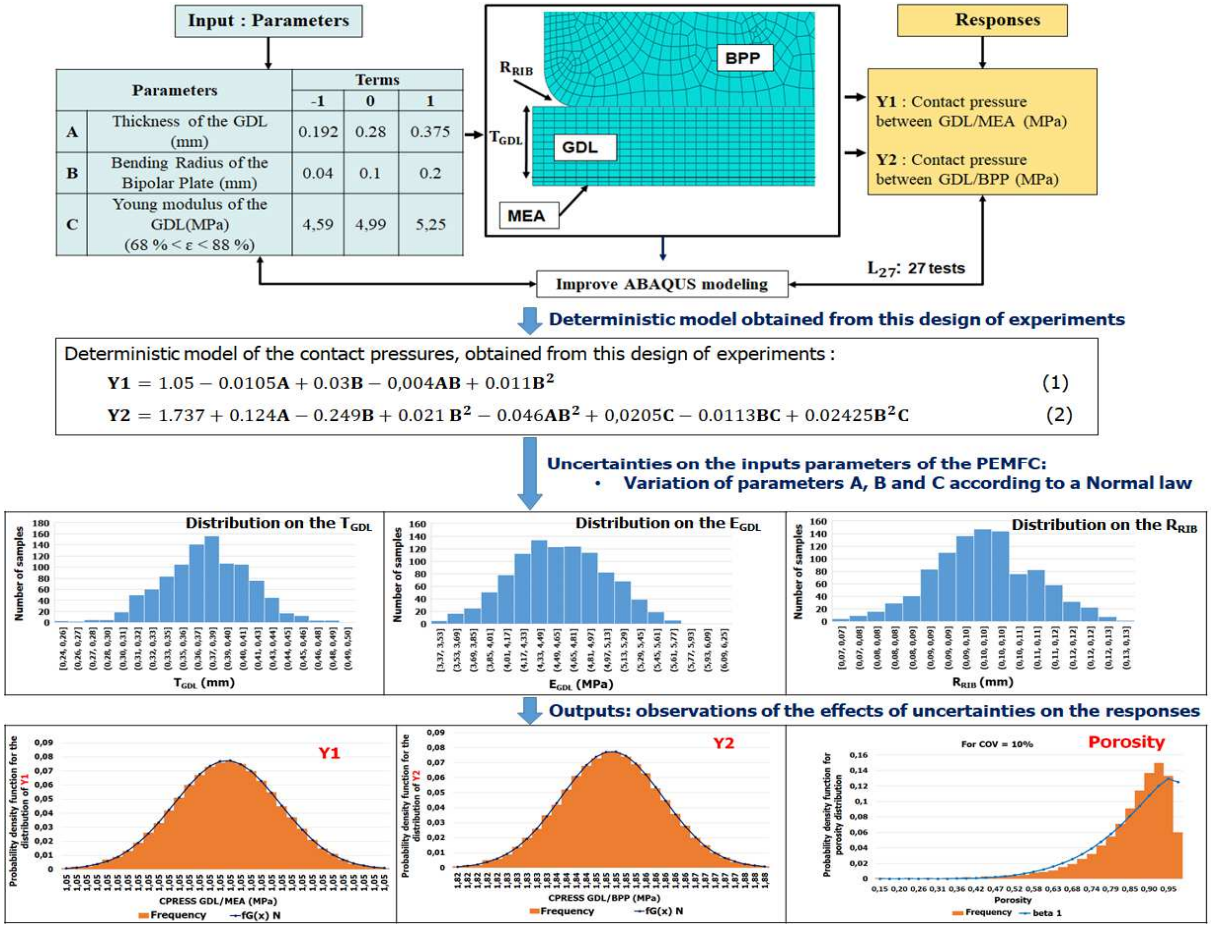

Figure 4: Schematic representation of the procedure for integrating uncertainties in the deterministic model.

After defining the approach to integrate uncertainties parameters in our model to study the effect of these distributions on the contact pressure distribution, we proceed to a statistical analysis of the responses. We consider the equations 1 and 2 of figure 4 which correspond respectively to the contact pressure between GDL/MEA (Y1) and GDL/BPP (Y2) and varying the input parameters (T_{GDL} parameter A, R_{RIB} parameter B and E_{eqv} parameter C) according to the normal law (which corresponds optimistic dispersion). Note that the normal law (Gauss) is represented by two shape parameters: an average value (m) of the studied parameter and the coefficient of variation of the studied parameter (COV). The COV is estimated by the ratio between the standard deviation and the average of the parameter studied as:

$$COV = \frac{\sigma}{m} \qquad (4)$$

3.1 Uncertainties on the input parameters

We have chosen a realistic dispersion of 10%. [3]. In order to define statistical distributions, 1000 numerical simulations were performed. This number was chosen to obtain a good agreement between the simulation time and the precision of the results. Table 1 shows the shape parameters (average and standard deviation) for each parameter.

Table 1: Shape parameters of the distribution of input parameters.

Input parameters	Average	Standard deviation	COV
T_{GDL} (A)	0,375 mm	0,0375	0,1
R_{RIB} (B)	0,1 mm	0,01	0,1
E_{eqvGDL} (C)	4,59 MPa	0,459	0,1

3.2 Results and discussion

3.2.1 Statistical distributions on the output parameters (Y1: CPRESS GDL/MEA and Y2: CPRESS GDL/BPP)

The distributions on the input parameters give to statistical distributions on the output parameters. Figures 5.a and 5.b respectively show the predicted distribution obtained of the contact pressure C_{PRESS} between GDL/MEA (Y_1) and GDL/BPP (Y_2).

For an uncertainty of 10% on the Y1 and Y2, and based on the theory of K. Pearson on the probability surfaces [18], we can noted that for 1000 numerical simulations:

1. The distribution of the Y_1 response (C_{PRESS} GDL/MEA) is numerically modeled by a Gauss's law with an average of 1.049 MPa with a dispersion of 0.32.

2. Similarly, the response of Y_2 (C_{PRESS} GDL/BPP) also attends a Gauss's law with an average of 1.849 MPa and a dispersion of 0.32.

As already shown in Figure 3, the contact resistance decreases in function of the clamping pressure. A model has been developed showing the relationship between the interfacial resistance and the clamping pressure and it is illustrated as follows: $R_{GDL/BPP} = 3.2973 * P^{-0.532}$ [16].

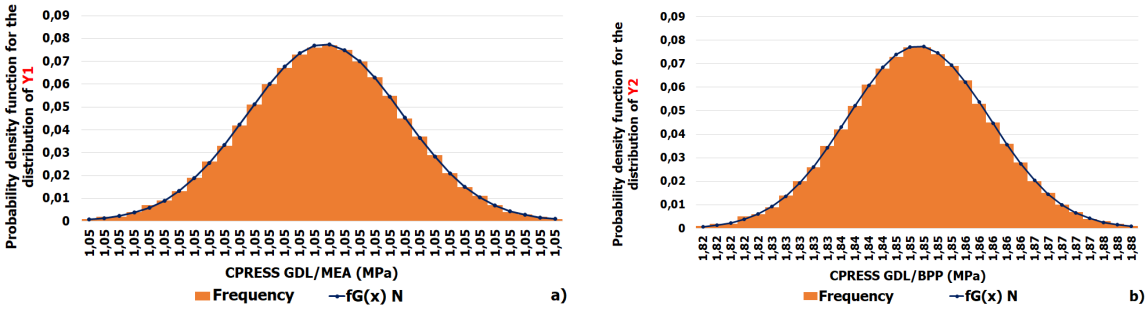

Figure 5: Probability density function for the distribution of: a) Y_1 and b) Y_2

By varying the clamping pressure according to a normal law with an average of P = 1 MPa and a COV of 10%, the contact resistance between GDL/BPP attends a beta 1 law (Figure 6.a). The obtained results show that the coefficient of variation of the electrical resistance $R_{GDL/BPP}$ is 0.39 with a minimum of 2.88 and a maximum of 4 $m\Omega.cm^2$. Therefore, we noted that for different clamping pressures that vary according to a normal law with a dispersion of 10%, we find that the contact resistance between GDL/BPP follows a Beta 1 law (Figure 6b). Figure 6.b shows the distribution of $R_{GDL/BPP}$ as a function of clamping pressure with the shape parameters (lower and upper) for each clamping pressure. In addition, Table 2 shows the shape parameters of beta 1 law (min*, max* and average) for each clamping pressure.

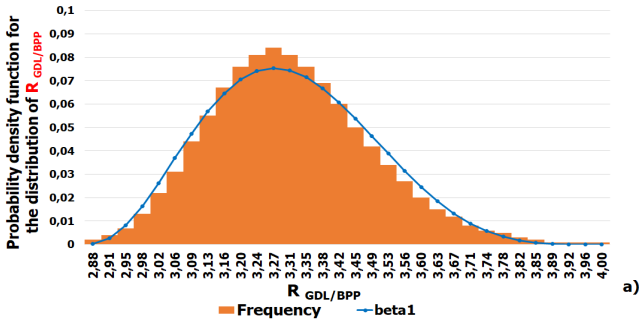

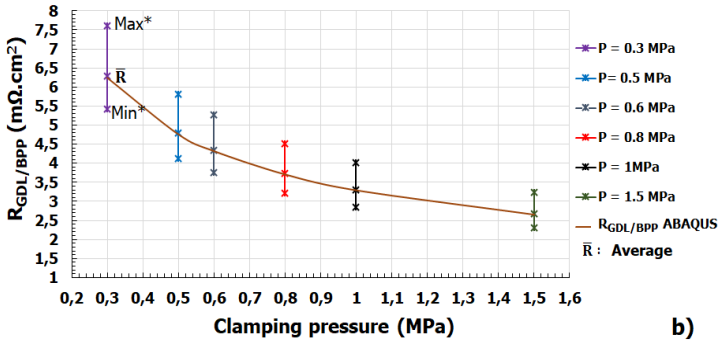

Figure 6: a) Probability density function for the distribution of $R_{GDL/BPP}$ and b) shape parameters (lower (Min*), upper (Max*) and Average ($\bar{R}$)) for each clamping pressure.

Table 2: Shape parameters of the distribution of $R_{GDL/BPP}$.

Clamping pressure P (MPa)	$R_{GDL/BPP}$ (mΩ.cm^2)			
	Min*	Max*	Average	Predicted Average
0.3	5.38	7.99	6.28	6.25
0.5	4.2	5.96	4.78	4.77
0.6	3.76	5.18	4.34	4.33
0.8	3.25	4.58	3.73	3.71
1	2.88	4	3.31	3.29
1.5	2.29	3.22	2.67	2.66

3.2.2 Physical explanation for the distribution of two responses (Y_1, Y_2)

We provide the explanation about the shape of distribution observed at the level of two studied responses. For the two responses (Y_1 and Y_2), we can noted that the increase in the input dispersion (from 1 to 10%) leads to the same output distribution whose shape attends the Gauss's law (see Figure 7).

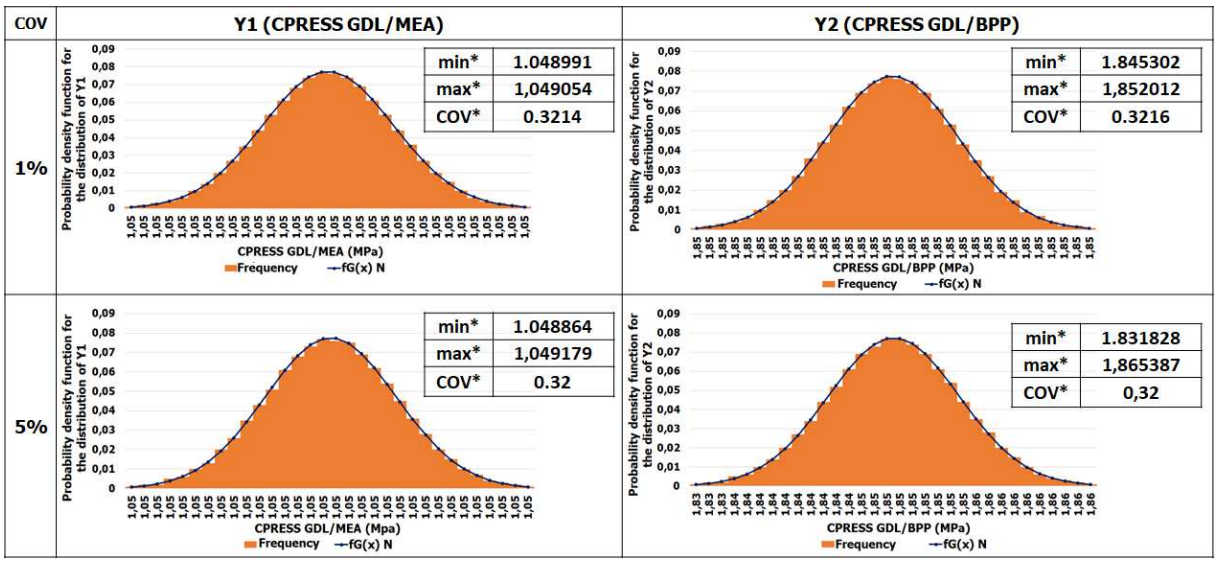

Figure 7: Probability density function for the distributions of contact pressures Y1 and Y2 for two input distributions: 1 and 5%.

As the contact pressure (Y_1 and Y_2) are function of the mechanical parameters, and in particular the Young's modulus of the GDL E_{eqv}, so the porosity of the GDL is the main

parameter of the variation of the shape of the output distribution. By varying the E_{eqv} according to a normal law, Figure 8 shows that the porosity of the GDL follows a beta 1 law. The increase in the input dispersion (from 1 to 5 then 10%) on the E_{eqv} leads to an output distribution (porosity of the GDL), which the shape approaches more and more than beta 1 law (Figure 8).

We can noting that, the variation of the porosity of the GDL (low, high) leads to a modification of the geometry of the two components (GDL and MEA) (see Table 3), and consequently, to a no-uniform distribution of the C_{PRESS} between the different components of the PEMFC. Also, as the porosity of the GDL and the geometries of the cell components depend on the clamping pressure, which itself also influences the contact between the cell components, this physically means that the distribution of the contact pressure between GDL/MEA (Y1) and GDL/BPP (Y2) is influenced by the distribution of the porosity of the GDL. With the same conditions, the increase in the COV of the porosity from 1 to 10% leads to an increase in the zone of variation of the porosity (Figure 9):

- Between [84% ; 90 %] for a dispersion of 1%
- Between [55% ; 97 %] for a dispersion of 5%
- Between [10% ; 97 %] for a dispersion of 10%

Following these variations, we can noted that a porosity with a dispersion of 5% has an acceptable variation range in comparison with those observed in the literature.

It can also see that the porosity has advantages as well as inconveniences on the contact pressures. In fact, when the GDL is deformed under the clamping pressure, the porosity and permeability decrease and are distributed in a non-uniform way. Therefore, the identification of the range of the porosity variation is required in order to avoid:

- The drying and submersion of the membrane, which influence the distribution of contact pressure between GDL/MEA (Y_1).
- The flooding phenomena of the GDL and the reduction of the contact area at the interface which influence the distribution of contact pressure between GDL/BPP (Y_2).

We know that water flooding is one of the major problem affecting the performance of the fuel cell. Therefore, the optimization of mechanical parameters such as the geometry of the bipolar plate, the thickness of the porous media (GDL) as well as its porosity is considered the most suitable method for operate the flooding phenomena.

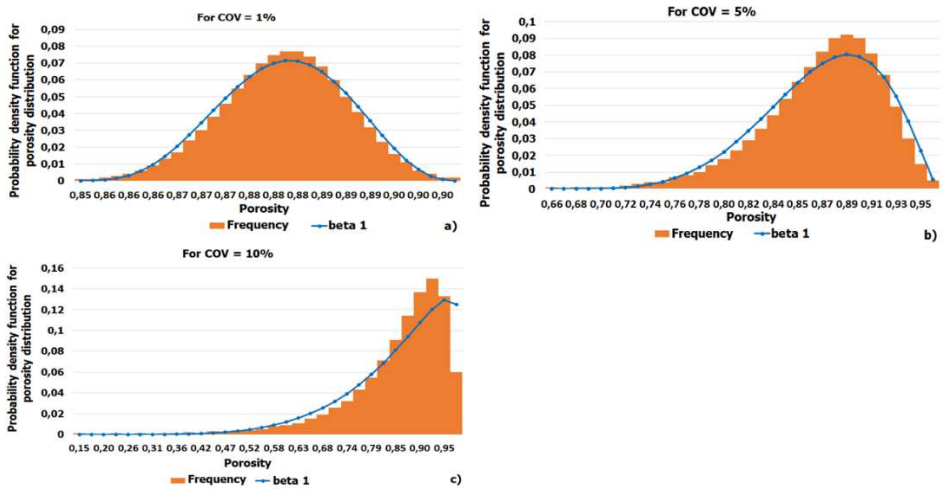

Figure 8: Probability density function for the distribution of the porosity of the GDL for three coefficients of variation: a) 1%, b) 5% and c) 10%.

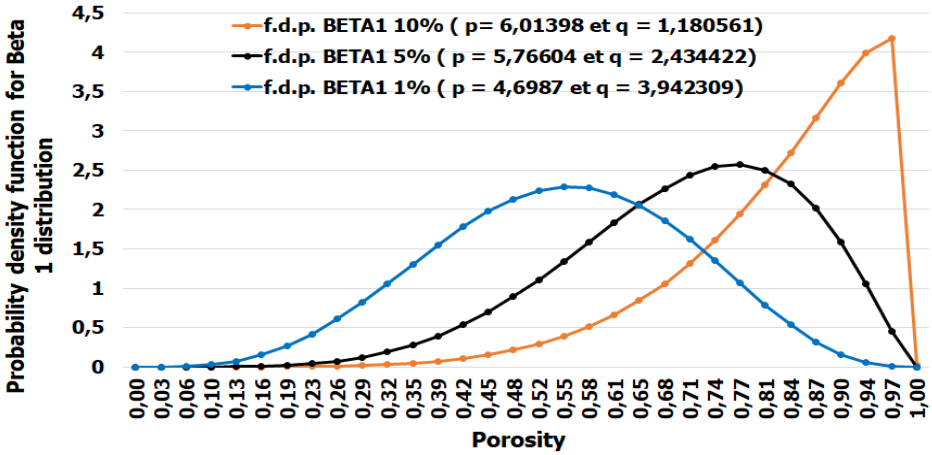

Figure 9: Interval of variation of the porosity of the GDL for three coefficients of variation 1, 5 and 10%.

Table 3: Advantages and disadvantages of the porosity of the GDL on the distribution of the contact pressure Y1 and Y2.

	Advantages	Disadvantages
High Porosity 88%	1. Increase the mass transport in the cell 2. Accelerate the reactive gases circulation towards the electrode 3. Accelerate the evacuation of the water 4. Avoid the flooding phenomena in the GDL while maintaining the membrane in a well hydrated state which causes favorable conditions for the electrochemical reaction.	1. Block the elimination of water from the GDL: the excess water will accumulate through the electrodes, and will block the porous layers which affect the state of contact between GDL/BPP and GDL/MEA 2. Lead to an "invasion" at high current densities [19, 20, 21].Therefore this increase has a certain limit.
		3. Increase the fraction of the pores and decreases the solid fraction: This increase in the fraction of the pores leads to an increase in the concentration of stresses around the pores, which leads to localization of the stresses.

		4. Cause a decrease in the Young's modulus E_{eqv} which then causes a decrease in the toughness of the material of the GDL. 5. Cause a reduction in the active area available for the electrochemical reaction: This reduction of the active surface increases the contact resistance and therefore the power density of the PEMFC decreases.
Low porosity 10%	1. Decrease the interfacial electrical resistance between GDL/BPP. 2. Avoid the flooding of the GDL 3. Promotes hydration of the membrane.	1. Can dry the membrane and even cause it to rupture [22] 2. Make the membrane permeable to gases by causing overheating allowing a dysfunction in the fuel cell system.

We have seen in figure 5 that, the two responses Y_1 (C_{PRESS} GDL/MEA) and Y_2 (C_{PRESS} GDL/BPP) are random, this means that there are bad and good situations. Since there are bad situations, such as the problem of flooding of water in the GDL, problem of gas leak and problem of deformation of the components of the fuel cell, in this case we search to study the influence of random inputs on random outputs in order to avoid these different problems.

In order to determine the incidence of different dispersions of the porosity in the GDL, as well as other mechanical parameters on the contact pressures between GDL/MEA and GDL/BPP, stochastic study is performed via a numerical design of experiment.

3.3 Stochastic study performed via a numerical Design of Experiment

The parameters A, B and C varies according to a normal law of average and coefficient of variation with two modalities for each parameter. Complete plan [23-24] is used to realize the 64 experiments and for each experiment 1000 numerical simulations is carried out. The value of the contact pressure is calculated using deterministic model already validated previously. The Terms of the different input parameters are shown in Table 4.

The responses studied are C_{PRESS} GDL/MEA and C_{PRESS} GDL/BPP. The output distributions Y1 and Y2 are represented by their forms descriptors: the average, the coefficient of variation, the kurtosis, the skewness. The study can be perform with the various tools attached to the method of design of experiments. In the next paragraph, we establish the chart of the effects to study the impact of the input parameters on four forms of output of the statistical distribution of responses.

Table 4: Terms of the parameters of the numerical design of experiment

		Terms	
Input	Parameters	-1	1

T_{GDL} (mm)	mA	0,192	0,375
	COV A	1%	10%
R_{RIB} (mm)	mB	0,04	0,2
	COV B	1%	10%
E_{eqv} (MPa)	mC	4,59	5,25
	COV C	1%	10%

3.3.1 Analysis of the results of the design of experiment: Chart of the effects

a) Effect of the random input parameters on the Y_1 response: C_{PRESS} GDL/MEA

Figure 10 shows respectively the effects of parameters on the average, on the dispersion (COV), on the skewness and the kurtosis of the C_{PRESS} GDL/MEA. Regarding the chart of effect related to the average of C_{PRESS} GDL/MEA (Y_1) we could make the following observations:

1. The **COV C, mC, COV B** and **COV A** parameters have no impact on the average of the distribution of the contact pressure GDL/MEA. Therefore, these parameters do not modify the form of the distribution of Y1.
2. On the other hand, the average of the contact pressure between GDL/MEA is strongly influenced by the two parameters **mB** (average of the bending radius of the BPP) and **mA** (average of the thickness of the GDL). The increase in the parameter **mB** leads to an increase of the average of C_{PRESS} GDL/MEA by 86.3%. The decrease in the average of the GDL thickness (**mA**) results in an increase in the average of contact pressure GDL/MEA (mY_1). This increase in mY_1 improves the diffusion of reactive gases from the channels of the bipolar plate towards the membrane, which avoids the phenomena of drying of the membrane in which a greater amount of water promotes the hydration of the membrane.
3. The increase in dispersion on the **COV B** causes an increase in the dispersion of the C_{PRESS} GDL/MEA (31.75%). The increase in the average of the bending radius of the bipolar plate **mB** leads to an increase in the dispersion of Y_1 by 31.11%. This increase in the dispersion of the contact pressure GDL/MEA causes a deformation in the structure of the membrane (cracks, perforation of the membrane, etc.) resulting from the phenomena of drying and swelling of the membrane.

   Therefore, the membrane will expand or contract depending on its water load and therefore apply more or less pressure on the GDL. This pressure will modify the porosity of the porous media and therefore change the diffusion of gases through this element. The increase in the dispersion of the thickness of the GDL **(COV A)** leads to a decrease in the

dispersion of Y_1 by 4.11%.This decrease in the COV Y_1 leads to a decrease in the ohmic resistance in the membrane, which promotes hydration of the membrane.

4. The **COV C, mC** and **mA** parameters have no effect on the COV of the distribution of the C_{PRESS} GDL/MEA. This means that these three parameters do not change the shape of the output distribution (Y_1).
5. The skewness and kurtosis of Y_1 are strongly influenced by the same parameters influencing the dispersion of Y_1 and which are **mB** (the average of the bending radius of the bipolar plate), **COV B** (the dispersion of the bending radius of BPP)**.** The increase in the average and the dispersion of the bending radius of the bipolar plate leads to a small increase of:
   - The skewness of the C_{PRESS} GDL/MEA from -0.005 to 0.02 for the average mB (31.56%) and for the dispersion COV B (31.04%).
   - The kurtosis of the C_{PRESS} GDL/MEA from -0.093 to -0.0916 for the average mB (37.59%) and for the dispersion COV B (from 31.44%).

These different values of the skewness and the kurtosis are close to zero: This means that the skewness and the kurtosis confirm the fact that the distribution of the contact pressure between GDL/MEA (Y_1) follows the distribution of the input parameters (Gauss's law). The statistical equations showing the relationship between these four shape parameters (m Y_1, COV Y_1, skewness of Y_1 and kurtosis of Y_1) and the most significant input parameters as well as the interactions are presented in section 3.3.2 below.

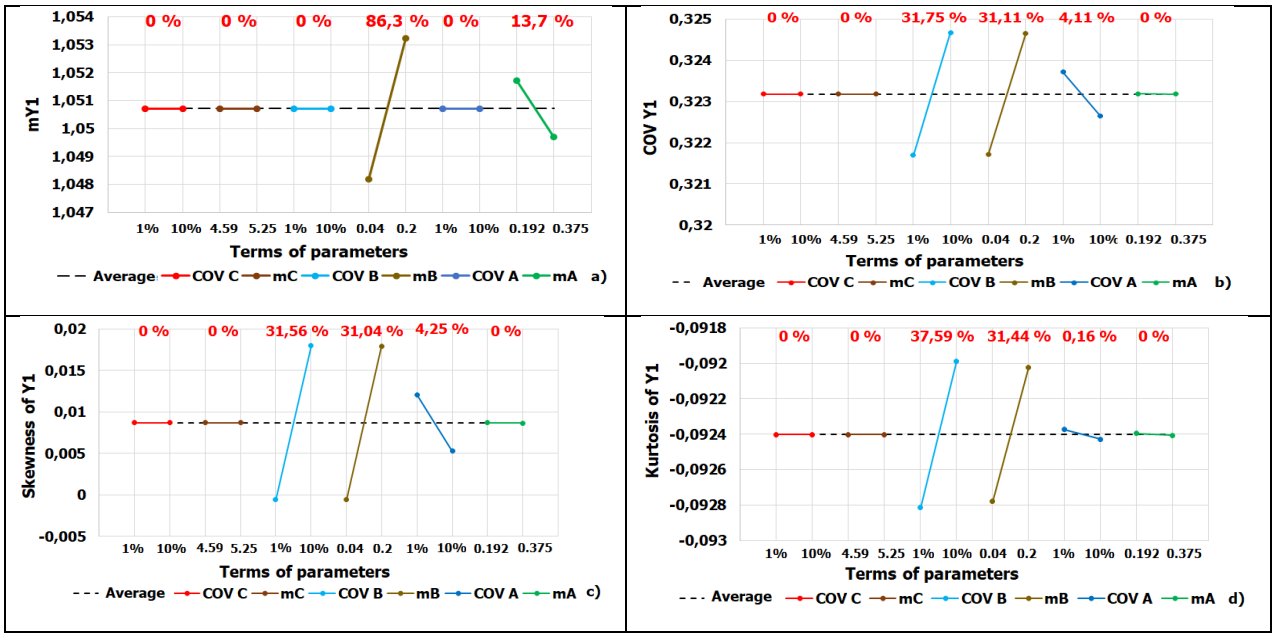

Figure 10: Chart of the effects of the random input parameters on the contact pressure between GDL/MEA (Y_1): a) average b) the covariance c) skewness and d) kurtosis.

- *Effect of the random input parameters on the Y_2 response: C_{PRESS} GDL/BPP*

Figure 11 shows respectively the effects of parameters on the average, on the dispersion (COV), on the skewness and the kurtosis of the C_{PRESS} GDL/BPP. Regarding the chart of effect related to the average of C_{PRESS} GDL/BPP we could make the following observations:

1. The coefficient of variation of the input parameters has no influence on the average C_{PRESS} GDL/BPP. This seems logical since in Figure 7, we found that increasing the dispersion on the input parameters contributes to the same shape distribution of the outputs.
2. The increase in Young's modulus **(mC)** from 4.59 to 5.25 MPa, which corresponds respectively to a porosity of 88 and 68%, has a positive effect on the C_{PRESS} GDL/BPP. A porosity of 68% increases the toughness of the material of the GDL, which avoids the flooding phenomena in the porous GDL.
3. A high influence of the average of the bending radius of the bipolar plate **mB** (74%) is observed. The increase in mB from 0.04 to 0.2mm leads to a decrease in mY_2. This decrease in mY_2 causes a decrease in the active surface available for the electrochemical reaction, which increases the C_{PRESS} GDL/BPP and consequently, a decrease in the power density of the fuel cell.
4. The increase in the thickness of the GDL **(mA)** leads to an increase in the C_{PRESS} GDL/BPP by 19.5%. This increase results in a decrease in contact resistance and an improvement in PEMFC performance. This is logical, since the type of GDL used is TORAY TGP-H-120 and several experimental studies have shown that GDL of type GP-H-120 has the lowest contact resistance.
5. The increase in dispersion on the input parameters **(COV B)** leads to an increase in the dispersion of the C_{PRESS} GDL/BPP by 9.5%. The increase in the dispersion of the thickness of the GDL **(COV A)** leads to a small increase in the dispersion of the C_{PRESS} GDL/BPP by 0.76%. The increase in the average of the **mB** leads to an increase in the dispersion of the contact pressure Y_2 by 4.12%.
6. The **mA** has no effect on the distribution of the COV of the CPRESS GDL/BPP.
7. The increase in the dispersion on the Young's modulus of the GDL **(COV C)** leads to a decrease in the dispersion of C_{PRESS} GDL/BPP by 8.22%. Statistically, this effect is considered significant. As explained before in Figure 9, a dispersion of 10% of the porosity of the GDL leads to an increase in the variation interval of the porosity [10; 97%]. This interval has an inconvenient when the porosity of the GDL decreases below 40% then causing an insufficient supply of the reactive gases: the water

produced by the electrochemical reaction won`t be evacuated which leads to a flood in the porous media (GDL), which affects the C_{PRESS} GDL/BPP.

In addition, a dispersion of 1% of the porosity of the GDL increases the coefficient of variation of C_{PRESS} GDL/BPP with a porosity variation interval of [84; 90%]. This low variation interval has a negative effect such that a high porosity can block the elimination of water from the GDL and therefore lead to a flooding at high current densities. Therefore, a dispersion of 5% (between 1 and 10%) in which the porosity varies in an interval [55; 97%] seems the most reliable for long lifetime of the PEMFC. This explains the influence of the average of the Young's modulus **(mC)** on the COV Y_2. A Young's module of E_{eqv} = 5.25 MPa corresponding to a porosity of 68% reduces the COV Y_2 by 0.36%.

As this porosity (68%) is between the intervals of variation of the dispersion porosity of 5% (see figure 9), this means an improvement of the mass transport and reduction of its losses, acceleration of the circulation of the reactive gases towards the electrode.

8. The six parameters influence in the same way the two shape parameters (skewness and kurtosis) of the Y_2 response. This confirms the fact that the distribution of the C_{PRESS} GDL/BPP follows the distribution of the input parameters.
9. The COV C (8.21%), COV B (11.9%) and mB (6.46%) parameters are the most significant on the skewness of Y_2. Statistically, the other parameters do not appear to be significant. We can see that the variation of the modalities between the lower level and the upper level causes a variation of the skewness of Y_2 between -0.01 and 0.07.
10. The COV B (7.31%) and mB (5.25%) parameters are the most significant on the kurtosis of Y_2. Statistically, the other parameters do not appear to be significant. Increasing COV B from 1 to 10% and mB from 0.04 to 0.2mm leads to an increase in the kurtosis of Y_2 from -0.094 to -0.069. We can see that these different values of the skewness and the kurtosis are close to zero: This means that the skewness and the kurtosis confirm the fact that the distribution of the C_{PRESS} GDL/BPP follows the distribution of the input parameters (Gauss's law).

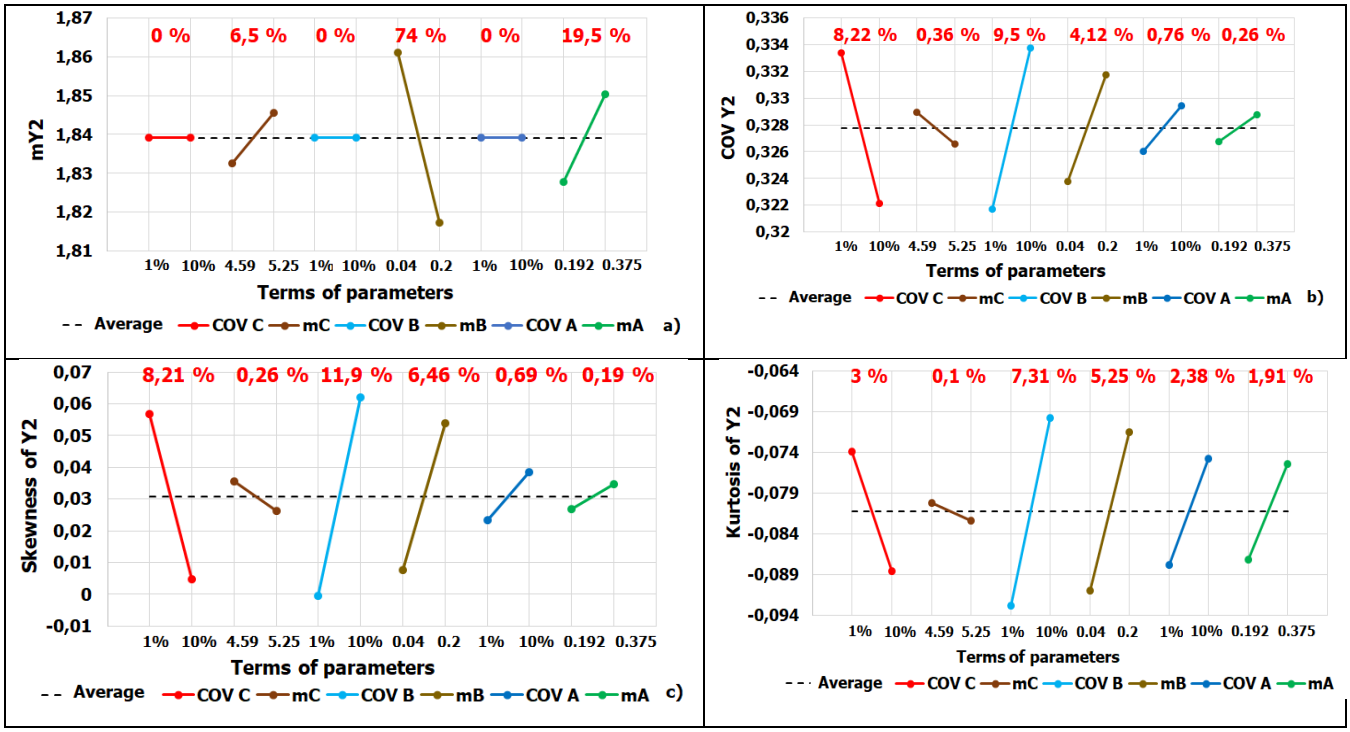

Figure 11: Chart of the effects of the random input parameters on the contact pressure between GDL/BPP (Y_2): a) average b) the covariance c) skewness and d) kurtosis.

The statistical equations showing the relationship between these four shape parameters (mY_2, COV Y_2, skewness of Y_2 and kurtosis of Y_2) and the most significant input parameters as well as the interactions are presented in section 3.3.2 below.

Before presenting the statistical models showing the relations between the random input parameters and the outputs (Y_1 and Y_2), we will present in Table 5 the synthesis of the results of the chart of effects resulting from the design of experiments. As already mentioned previously, the outputs are random, this means, that there are bad and good situations of Y_1 and Y_2. As there are a bad efficience (like the problem of flooding of water in the GDL, problem of gas leak and problem of deformation of the components of the fuel cell by appearance of cracks), in this case, we are looking to see how we can choose random input parameters to avoid these bad situations. From the results of the design of experiments (chart of effects), we show in Table 5 the modalities of the random input parameters corresponding to each of the bad and good situations. The increase in the thickness of the GDL, the decrease in the bending radius of the BPP and the increase in the Young's modulus of the GDL with a dispersion of 5% make it possible to avoid the various problems corresponding to the bad situations.

Table 5: Random input parameters effect on the fuel cell efficiency.

Y1 and Y2 Situations	Bad efficience	Good efficience

Input parameters			
mA	T_{GDL} = 0.192 mm - Prohibit the circulation of reactive gases from the channels of the bipolar plate to the membrane		**T_{GDL} = 0.375 mm** - Enhances the evacuation of liquid water and avoid the flooding phenomenon in the GDL
mB	R_{RIB} = 0.2 mm - Decreases the contact area between the bipolar plate and the GDL		**R_{RIB} = 0.04 mm** - Increases the contact area available for the electrochemical reaction
mC	E_{eqv} = 4.59 MPa - Corresponds to a porosity of 88%, - This level of the porosity causes a decrease in the modulus of elasticity and therefore a decrease in the toughness of the GDL material.		**E_{eqv} = 5.25 MPa** - Corresponds to a porosity of 68%, - Enhances the circulation of reactive gases towards the electrode and the evacuation of the water produced by the electrochemical reaction.
COV C	1%	- Porosity of the GDL between [84; 90%]. - This small range of variation can block the elimination of water from the GDL and therefore lead to a flood in the porous media (GDL).	A **dispersion of 5%** (between 1 and 10%) in which the porosity varies in a range [55; 97%] appears to be the most reliable for the variation of contact pressures.
	10%	- Porosity of the GDL between [10; 97%]. - Causes insufficient circulation of reactive gases, which affects the contact between GDL/BPP.	

3.3.2 Statistical model of responses according to the parameters studied

After calculating and interpreting the effects of the parameters studied, as well as their interactions, statistical models of the responses Y1 et Y2 are proposed from the design of experiment presented previously. We will give the equations of the average, the coefficient of variation, the skewness and the kurtosis of two outputs:

- For the response Y_1 (C_{PRESS} GDL/MEA):

$$\mathbf{m_{Y1}} = 1{,}050717 + 0{,}002521 * \mathbf{mB} - 0{,}001 * \mathbf{mA} \quad (5)$$

$$\mathbf{COV_{Y1}} = 0{,}3232 + 0{,}00149 * \mathbf{COV\ B} + 0{,}00147 * \mathbf{mB} + 0{,}00143 * \mathbf{COVB} * \mathbf{mB} \quad (6)$$

$$\mathbf{Skewness}_{\mathbf{Y1}} = 0{,}00869 + 0{,}00929 * \mathbf{COV\ B} + 0{,}00921 * \mathbf{mB} + 0{,}00893 * \mathbf{COVB} * \mathbf{mB} \quad (7)$$

$$\mathbf{Kurtosis}_{\mathbf{Y1}} = -0.0924 + 0{,}00041 * \mathbf{COV\ B} + 0{,}00038 * \mathbf{mB} + 0{,}00037 * \mathbf{COVB} * \mathbf{mB} \quad (8)$$

Equations 5 and 6 show that the coefficients multiplied by the input parameters (mB, mA and COVB) as well as the interactions between these parameters are close to zero. This means that

by varying these input parameters with a dispersion between 1 and 10%, we have a dispersion of 32% for Y_1 with an average of 1.05 MPa. Equations 7 and 8 show that all the coefficients are close to zero (skewness and kurtosis of $Y_1 = 0$), this confirms the fact that the distribution of Y_1 follows the normal law.

- For the response Y_2 (C_{PRESS} GDL/BPP):

$$\mathbf{m_{Y2}} = 1{,}8391 + 0{,}00648 * \mathbf{mC} - 0{,}0219 * \mathbf{mB} + 0{,}01126 * \mathbf{mA} \quad (9)$$

$$\mathbf{COV_{Y2}} = 0{,}3277 - 0.0056 * \mathbf{COV\ C} + 0.00603 * \mathbf{COV\ B} - 0.0056 * \mathbf{COV\ C} * \mathbf{COV\ B} - 0.0044 * \mathbf{COV\ C} * \mathbf{mB} * \mathbf{COV\ A} - 0.0045 * \mathbf{COV\ C} * \mathbf{COV\ B} * \mathbf{mB} * \mathbf{COV\ A}$$
(10)

$$\mathbf{Skewness_{Y2}} = 0{,}031 - 0.026 * \mathbf{COV\ C} + 0.031 * \mathbf{COV\ B} - 0.0256 * \mathbf{COV\ C} * \mathbf{COV\ B} + 0.023 * \mathbf{mB} + 0.023 * \mathbf{COV\ B} * \mathbf{mB} - 0.0208 * \mathbf{COV\ C} * \mathbf{mB} * \mathbf{COV\ A} - 0.0212 * \mathbf{COV\ C} * \mathbf{COV\ B} * \mathbf{mB} * \mathbf{COV\ A}$$
(11)

$$\mathbf{Kurtosis_{Y2}} = -0.0813 + 0.01149 * \mathbf{COV\ B} + 0.00974 * \mathbf{mB} + 0.0097 * \mathbf{COV\ B} * \mathbf{mB} - 0.0095 * \mathbf{COV\ C} * \mathbf{mB} * \mathbf{COV\ A} - 0.0095 * \mathbf{COV\ C} * \mathbf{COV\ B} * \mathbf{mB} * \mathbf{COV\ A}$$
(12)

Equation 10 shows that the coefficients multiplied by the input parameters (COV C, COV B, COV A and mB) as well as the interactions between these parameters are close to zero. This means that by varying these input parameters with a dispersion between 1 and 10%, we have a dispersion of 32% for the C_{PRESS} between GDL/BPP.

Equation 12 shows that the coefficients multiplied by the input parameters (COV C, COV B, COV A and mB) as well as the interactions between these parameters are close to zero. We have a kurtosis coefficient close to zero (0.0813); this shows that the distribution of Y_2 follows the normal law.

The models generated (describing the distribution of Y_1 and Y_2) make it possible to present in a synthetic way the results obtained after various simulations related to the model. These statistical models could then be easily implemented in the context of reliability studies.

The stochastic study (design of experiments), presented in section 3.3.1 and 3.3.2, gave us ideas on the relation between the contact pressures between GDL/MEA (Y1) and GDL/BPP (Y2) with the random input parameters (equations 5 - 12). So it is necessary to validate these statistical models with the finite element analysis results using ABAQUS software.

3.3.3 Validation of statistical models resulting from the stochastic study

In order to validate these statistical models, FEA is performed using Abaqus software by setting the modalities of the input parameters to zero (see Table 6).

Table 6: Terms of the parameters of the experiment

Parameters		Terms
		0
T_{GDL} (mm)	mA	0.2835
	COV A	5.5%
R_{RIB} (mm)	mB	0.12
	COV B	5.5%
E_{eqv} (MPa)	mC	4,92
	COV C	5.5%

By setting the modalities of the input parameters to zero, the statistical models of two responses Y_1 and Y_2 resulting from the stochastic study performed through a numerical design of experiments give the values of the forms of output (average, coefficient of variation, Skewness and Kurtosis) of the distributions (Y_1 and Y_2).

In order to guarantee the Gaussian nature of the distribution of the contact pressure, 1000 numerical simulations are done by varying the input parameters according to the normal law with a zero terms of the parameters (see Table 6). Figures 12.a and b show respectively the numerical distribution of the contact pressure Y1 and Y2.

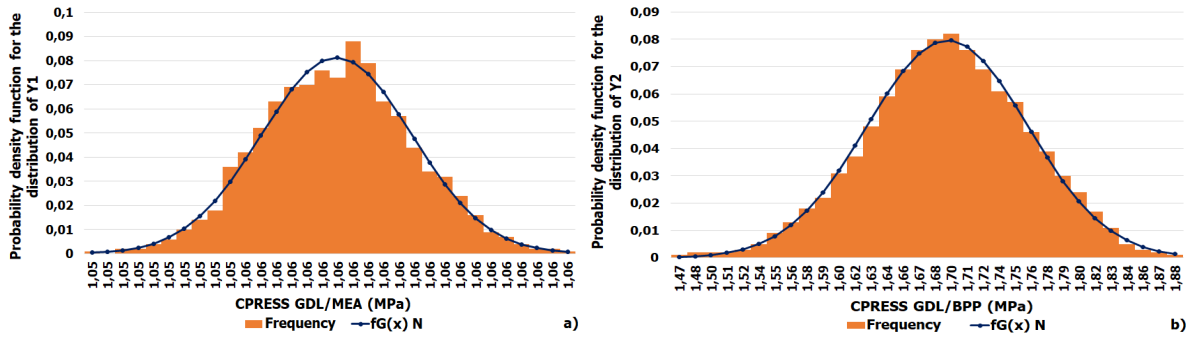

Figure 12: Distributions obtained on: a) Y_1 and b) Y_2.

Based on the theory of K. Pearson on the probability surfaces [18], we note that:

- Following the 1000 numerical simulations, the distribution of the Y_1 response is numerically modeled by a statistical Gauss's law with an average of 1.0568 MPa and a dispersion of 0.2984.
- Similarly, the response of Y_2 also attends a Gauss's law with an average of 1.6928 MPa and a dispersion of 0.2901.

The values obtained on the form descriptors of the distribution of contact pressure were compared with the values of design of experiments. Tables 7 and 8 respectively show the comparison between the results of the design of experiments and the numerical results. From Table 7, we note that the predicted results are close to the results of the design of experiments: a good correlation is observed for the average of Y_1 ($\mathbf{m_{Y1}}$). A little difference of 8% is observed in the coefficient of variation of Y_1 ($\mathbf{COV_{Y1}}$). At the level of the Skewness and Kurtosis of Y_1, low values (close to zero) were observed, this confirms the fact that the distribution of the Y_1 follows the normal law.

From Table 8, we note a little difference of 8.6% for the average of Y2 ($\mathbf{m_{Y2}}$): this difference is due to the small thickness of the GDL (T_{GDL} = 0.23 mm). We have seen in Figure 11.a that the decrease in the thickness of the GDL decreases the contact pressure between GDL/BPP. Likewise, compared to response Y_1, a little difference of 8% was observed for the coefficient of variation of Y_2 ($\mathbf{COV_{Y2}}$). For the Kurtosis of Y_2, a low value (close to zero) was observed (-0.0041), this confirms the fact that the distribution of the contact pressure between Y_2 follows the normal law. For the Skewness of Y_2, a negative value was observed (-0.1469) comparing with that of the value of the design of experiments (0.0308).

Table 7: Comparison between the design of experiments and numerical results on the form descriptors of the distribution of Y_1

Form descriptors	Design of experiments	Numerical
$\mathbf{m_{Y1}}$	1.050717	1.0568297
$\mathbf{COV_{Y1}}$	0.3232	0.2984
$\mathbf{Skewness\ _{Y1}}$	0.00869	0.03457
$\mathbf{kurtosis\ _{Y1}}$	-0.0924	-0.0818

Table 8: Comparison between the design of experiments and numerical results on the form descriptors of the distribution of Y_2

Form descriptors	Design of experiments results	Numerical
$\mathbf{m_{Y2}}$	1.8391	1.6928
$\mathbf{COV_{Y2}}$	0.3277	0.2901
$\mathbf{Skewness\ _{Y2}}$	0.0308	-0.1475
$\mathbf{kurtosis\ _{Y2}}$	-0.0813	-0.004013

4 Conclusion

In this study, a Design of Experiments was performed in order to study the effects of the uncertainties of the mechanical parameters on the contact pressures between the different components. Our results lead to the following main conclusions:
The distribution of the Y_1 (C_{PRESS} GDL/MEA) and Y_2 (C_{PRESS} GDL/BPP) responses is numerically modeled by a special statistical Gauss's law with a dispersion of 32%.

The parameters with the most effect on the contact pressure between GDL/MEA and contact pressure between GDL/BPP are bending radius of the bipolar plate of average 0.04 mm, thickness of the GDL of average 0.375 mm and Young's modulus of the GDL of average 5.25MPa.

A bending radius of the bipolar plate of average R_{RIB} = 0.04 mm and a thickness of the GDL of average T_{GDL} = 0.375 mm causes an increase in the average of the contact pressure between GDL/BPP, which results in a decrease in resistance contact between GDL/BPP.

By varying the Young's modulus of the GDL E_{eqv} according to a normal law, we observe that the porosity of the GDL follows a beta 1 law.
A stochastic study is performed through a numerical design of experiments in order to determine the impact of the different random parameters (porosity of the GDL, bending radius of the bipolar plate and thickness of the GDL) on the contact pressures between GDL/MEA and GDL/BPP. The results of the design of experiment show that:

- For the Y_1 response, the behavior of all the random input parameters is linear. The coefficient of variation, the Skewness and the kurtosis of Y_1 are influenced by the same parameters mB (the average of the bending radius of the bipolar plate), COV B (the dispersion of the bending radius of the BPP) as well as the interaction between these two parameters mB * COV B.
- For the Y_2 response, the behavior of all random input parameters is also linear. Statistical models of Y_1 and Y_2 responses resulting from the design of experiments show that by varying the input parameters with a coefficient of variation between 1 and 10%, we have a dispersion of 32% for the two responses Y_1 and Y_2. These static models of two responses are validated by the numerical simulation.

In this study, all these numerical simulations were performed with a particular modeling of clamping: a constant clamping pressure of P = 1MPa was imposed on the End plate. Moreover, the modeling of the thermo-electro-mechanical coupling was not taken into

consideration. In fact, it would be now interesting to study the influence of the temperature distribution on the electrical resistance of the fuel cell by considering the fully coupled thermo-electro-mechanical model.

References

[1] Charon, W., Iltchev, M. C., & Blachot, J. F. (2014). Mechanical simulation of a Proton Exchange Membrane Fuel Cell stack using representative elementary volumes of stamped metallic bipolar plates. *International Journal of Hydrogen Energy*, *39* (25), 13195- 13205.

[2] Vion-Dury, B. (2011). Mécanismes de vieillissement des électro-catalyseurs de pile à combustible de type PEMFC (Thèse de doctorat, Université de Grenoble, France).

[3] Coulon, R. (2012). Modélisation de la dégradation chimique de membranes dans les piles à combustibles à membrane électrolyte polymère (Thèse de doctorat, Université de Grenoble, France).

[4] Dafalla, A. M., & Jiang, F. (2018). Stresses and their impacts on proton exchange membrane fuel cells: A review. *International Journal of Hydrogen Energy*, *43* (4), 2327-2348.

[5] Akiki, T. (2011). Modélisation de la dégradation de la production de puissance d'une pile à combustible suite aux sollicitations mécaniques (Thèse de doctorat, Belfort-Montbéliard).

[6] Wasterlain, S. (2010). *APPROCHES EXPERIMENTALES ET ANALYSE PROBABILISTE POUR LE DIAGNOSTIC DE PILES A COMBUSTIBLE DE TYPE PEM* (Doctoral dissertation, Université de Franche-Comté).

[7] Massonnat, P. (2015). *Développement d'un modèle multi physique multidimensionnel de pile à combustible à membrane échangeuse de proton en temps réel pour système embarqué* (Doctoral dissertation, Université de Technologie de Belfort-Montbeliard).

[8] Zhang, L., Liu, Y., Song, H., Wang, S., Zhou, Y., & Hu, S. J. (2006). Estimation of contact resistance in proton exchange membrane fuel cells. *Journal of Power Sources*, *162*(2), 1165-1171.

[9] Kusoglu, A., Santare, M. H., Karlsson, A. M., Cleghorn, S., & Johnson, W. B. (2010). Numerical investigation of mechanical durability in polymer electrolyte membrane fuel cells. *Journal of the Electrochemical Society*, *157*(5), B705-B713.

[10] Vlahinos, A., & Kelkar, S. G. (2002). Designing for six-sigma quality with robust optimization using CAE. SAE Transactions, 1901-1908.

[11] Placca, L. (2010). *Impact des incertitudes sur le fonctionnement des piles à combustible par approche fiabiliste* (Doctoral dissertation, Thèse UTBM/CEA, soutenue le 17 décembre 2010).

[12] Noguer, N. (2015). *Aide à l'analyse fiabiliste d'une pile à combustible par la simulation* (thèse de doctorat à l'Université de Technologie de Belfort-Montbéliard).

[13] Mawardi, A., & Pitchumani, R. (2006). Effects of parameter uncertainty on the performance variability of proton exchange membrane (PEM) fuel cells. *Journal of power sources*, *160*(1), 232-245.

[14] Zhang, W., Cho, C., Piao, C., & Choi, H. (2016). Sobol's sensitivity analysis for a fuel cell stack assembly model with the aid of structure-selection techniques. *Journal of Power Sources*, *301*, 1-10.

[15] Akiki, T. (2011). Modélisation de la dégradation de la production de puissance d'une pile à combustible suite aux sollicitations mécaniques (Doctoral dissertation, Belfort-Montbéliard).

[16] Ouaidat, G., Cherouat, A., Kouta, R., & Chamoret, D. (2020). Numerical modeling of the mechanical behavior of proton exchange membrane fuel cell performance: Design of experiment study and optimization. *International Journal of Hydrogen Energy*, *45*(46), 25210-25226.

[17] Mishra, V., Yang, F., & Pitchumani, R. (2004). Measurement and prediction of electrical contact resistance between gas diffusion layers and bipolar plate for applications to PEM fuel cells. *Journal of Electrochemical Energy Conversion and Storage*, *1* (1), 2-9.

[18] J-L. Norman, S. Kotz, N. Balakrishnan, « Continuous Univariate Distributions », A Wiley-Interscience Publication, 1994, 791 pages. ISBN: 978-0-471-58495-7.

[19] Michel Broniatowski, Kom Gildas Hermann. Méthodes Form et Sorm. 2014. <hal-00966695v2>

[20] Movahedi, M., A. Ramiar, and A. A. Ranjber. "3D numerical investigation of clamping pressure effect on the performance of proton exchange membrane fuel cell with interdigitated flow field." Energy 142 (2018): 617-632.

[21] Das, Prodip K., Xianguo Li, and Zhong-Sheng Liu. "Analysis of liquid water transport in cathode catalyst layer of PEM fuel cells." International Journal of Hydrogen Energy 35.6 (2010) : 2403-2416.

[22] Jourdani, M. (2019). Simulation Numérique Couplée des Phénomènes Thermo- fluide, Electrochimique et Mécanique dans une Pile à Combustible type PEMFC (Thèse de

doctorat, Ecole Mohammadia d'Ingénieurs, Maroc)

[23] M. Pillet, « Les plans d'expériences par la méthode Taguchi », Paris : Les Ed. d'Organisation, 1999, c1997, ISBN : 2-7081-2031-X.

[24] J. Goupy, « La méthode des plans d'expériences : optimisation du choix des essais & de l'interprétation des résultats », Paris : Dunod, c1988, ISBN : 2-04-018732-4.

[25] Matera, S., Schneider, W. F., Heyden, A., & Savara, A. (2019). Progress in accurate chemical kinetic modeling, simulations, and parameter estimation for heterogeneous catalysis. *ACS Catalysis, 9(8), 6624-6647*.

[26] Savara, A., & Walker, E. A. (2020). CheKiPEUQ Intro 1: Bayesian parameter estimation considering uncertainty or error from both experiments and theory. *ChemCatChem*, *12*(21), 5385-5400.

[27] Walker, E. A., Ravisankar, K., & Savara, A. (2020). CheKiPEUQ Intro 2: Harnessing Uncertainties from Data Sets, Bayesian Design of Experiments in Chemical Kinetics. *ChemCatChem*, *12*(21), 5401-5410.

Nomenclature

GDL	Gas diffusion layer
BPP	Bipolar plates
R_{RIB}	Bending radius of the bipolar plates (mm)
T_{GDL}	Thickness of the GDL (mm)
$\varnothing_P$	Diameters of the pores of the GDL (mm)
E_{eqv}	Young's modulus of the GDL (GPa)
P	Clamping pressure [MPa]
ε	Porosity of the GDL
$R_{GDL/BPP}$	Electrical contact resistance between the GDL/BPP [mΩ.mm^2]
C_{press}	Contact pressure [MPA]
Y1	Contact pressure between GDL/MEA [MPa]
Y2	Contact pressure between GDL/BPP [MPa]
COV	Coefficient of variation

σ: Standard deviation

m Average

mA Average of the Thickness of the GDL

COV A Coefficient of variation of the Thickness of the GDL

mB Average of the bending radius of the bipolar plate

COV B Coefficient of variation of the bending radius of the bipolar plate

mC Average of the Young modulus of the GDL

COV C Coefficient of variation of the Young modulus of the GDL

fG(x) Probability density function

$\bar{R}$ Average

Table List

Figure Captions

Figure 1: a) stack of 3 cells; b) Distribution of the contact pressure between GDL/BPP all along the GDL line for the 3 cells.

Figure 2: Terms of the input studied parameters and responses.

Figure 3: Contact resistance versus clamping pressure comparison numerical model and experimental results [16-17]

Figure 4: Schematic representation of the procedure for integrating uncertainties in the deterministic model.

Figure 5: Probability density function for the distribution of: a) Y1 and b) Y2

Figure 6: a) Probability density function for the distribution of $R_{GDL/BPP}$ and b) shape parameters (lower (Min*), upper (Max*) and Average ($\overline{R}$)) for each clamping pressure.

Figure 7: Probability density function for the distributions of contact pressures Y1 and Y2 for

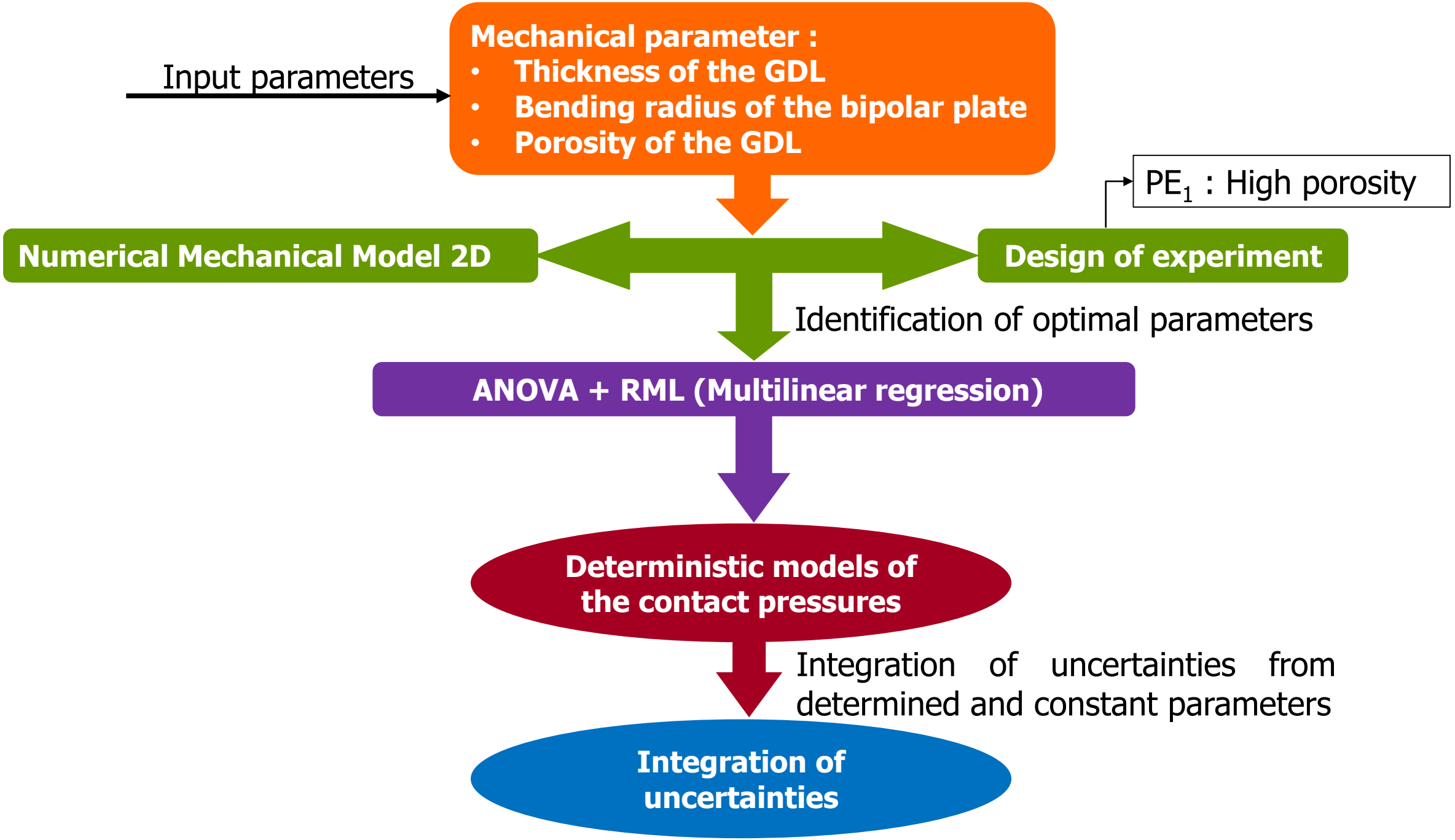
Input parameters
Mechanical parameter :
• Thickness of the GDL
• Bending radius of the bipolar plate
• Porosity of the GDL
PE1 : High porosity
Numerical Mechanical Model 2D
Design of experiment
Identification of optimal parameters
ANOVA + RML (Multilinear regression)
Deterministic models of the contact pressures
Integration of uncertainties from determined and constant parameters
Integration of uncertainties